

Origins of Uncertainty in the Response of the Summer North Pacific Subtropical High to CO₂ Forcing

Kezhou Lu¹, Jie He², and Isla Ruth Simpson³

¹Georgia Institute of Technology

²Georgia Tech

³National Center for Atmospheric Research (UCAR)

August 13, 2025

1 **Origins of Uncertainty in the Response of the Summer**
2 **North Pacific Subtropical High to CO_2 Forcing**

3 **Kezhou Lu¹, Jie He¹, and Isla R. Simpson²**

4 ¹School of Earth and Atmospheric Sciences, Georgia Institute of Technology, Atlanta, GA, USA

5 ²National Center for Atmospheric Research, Boulder, CO, USA

6 **Key Points:**

- 7 • Model spread in the response of the summer NPSH to CO_2 stems from model spread
8 in simulating tropical processes
9 • Model spread in tropical SST changes modulates the NPSH by influencing trop-
10 ical precipitation
11 • Model spread in tropical precipitation changes independent of model spread in SST
12 changes also adds to the uncertainty of the NPSH response

Corresponding author: Kezhou Lu, kezhou.lu@eas.gatech.edu

Abstract

The variability of the summer North Pacific Subtropical High (NPSH) has substantial socioeconomic impacts. However, state-of-the-art climate models significantly disagree on the response of the NPSH to anthropogenic warming. Inter-model spread in NPSH projections originates from models' inconsistency in simulating tropical precipitation changes. This inconsistency in precipitation changes is partly due to inter-model spread in tropical sea surface temperature (SST) changes, but it can also occur independently of SST uncertainty. Here, we show that both types of precipitation uncertainty influence the NPSH via the Matsuno-Gill wave response, but their relative impact varies by region. Through the modulation of low cloud fraction, inter-model spread of the NPSH can have a further impact on extra-tropical land surface temperature. The teleconnection between tropical precipitation and the NPSH is examined through a series of numerical experiments.

Plain Language Summary

The North Pacific Subtropical High (NPSH) is a semi-permanent high-pressure system located in the subtropical North Pacific. The variability in the summer NPSH has a significant impact on the monsoon and typhoons over East Asia and the hydroclimate of California. However, future projections of the NPSH using state-of-the-art climate models remain highly uncertain. By evaluating how much individual models deviate from the multi-model mean at different locations, we find four hot spots of high uncertainty in NPSH projections. Our analysis further reveals that the primary source of model variance in changes in the NPSH is tropical precipitation, which can be attributed to both inter-model SST-driven and non-inter-model SST-driven factors. Through numerical experiments, we demonstrate that the teleconnection between tropical precipitation and the NPSH is achieved through wave propagation.

1 Introduction

The North Pacific Subtropical High (NPSH) plays a crucial role in shaping the hydroclimate in the North Pacific, East Asia and North America. As part of the subtropical stationary wave system, the NPSH reaches its peak magnitude in the boreal summer ranging from $15^{\circ}N$ to $45^{\circ}N$ with its western branch extending to East Asia and eastern branch bordering North America (Wills et al., 2019). The western flank of the NPSH (WNPSH) transports moisture from the ocean to East Asia and the Indochina Peninsula, strengthening the Meiyu-Baiu rainfall and causing typhoons and floods (B. Wang et al., 2013; S. Zhou et al., 2019; Y. Wang et al., 2022). Meanwhile, the west coast of North America experiences warm and dry summers under the influence of the eastern flank of the NPSH (Burls et al., 2017; Seager et al., 2019). The response of the NPSH to anthropogenic warming is expected to significantly impact regional climates (Wills et al., 2019; Seager et al., 2019; J. Choi et al., 2016; W. Choi & Kim, 2019); therefore, reliable future projections of the NPSH are crucial for preparing adaptation plans.

State-of-the-art climate models participating in the fifth and sixth phases of the Coupled Model Intercomparison Project (CMIP5 and CMIP6) exhibit diverging responses of the summer NPSH under global warming (Li et al., 2012; Sigmond et al., 2007; C. He & Zhou, 2015; X. Chen et al., 2020; D. Huang et al., 2022; Park & Lee, 2021). The explanations for models' poor agreement on the summer NPSH projections can be broadly categorized into local and remote processes. Local contributors include subtropical land-sea moist static energy (MSE) contrast and subtropical sea surface temperature (SST) (Lindzen & Nigam, 1987). For example, Shaw and Voigt (2015) and Baker et al. (2019) proposed that the opposing effects of CO_2 induced land-sea MSE contrast and subtropical SST warming result in a weak and insignificant NPSH response. In addition, model differences in the NPSH response are also attributed to the inter-model spread in the pattern of SST changes over the subtropical oceans (P. Huang et al., 2013; Levine & Boos,

63 2019). Furthermore, previous studies have demonstrated that the model differences in
64 simulating East Asian summer monsoons (Rodwell & Hoskins, 2001; S. Zhou et al., 2019),
65 the surface sensible heating over the Tibetan Plateau (Duan et al., 2017), and subgrid-
66 scale topography (Boos & Hurley, 2013) also impact the NPSH projections.

67 Of all the remote factors contributing to uncertainties in the projections of the NPSH,
68 model differences in the response of tropical precipitation is suggested to play a signif-
69 icant role (Baker et al., 2019; X. Chen et al., 2020; M. Chen et al., 2019; Park & Lee,
70 2021). Based on stationary wave theory, the summer subtropical highs are maintained
71 by tropical and continental monsoon heating (e.g., Gill (1980); Ting et al. (2001); Rodwell
72 and Hoskins (2001)). Therefore, model uncertainties in tropical diabatic heating could
73 potentially propagate into the NPSH region as planetary Rossby waves and interact with
74 the NPSH. The inter-model spread of tropical precipitation is shown to be connected to
75 the tropical SST through convection processes (Xie et al., 2010a). For example, X. Chen
76 et al. (2020) demonstrated that the model uncertainty in projecting the WNPSH is linked
77 to inter-model spread of tropical SST, which involves a negative shortwave-convection-
78 SST feedback. Specifically, a positive SST anomaly in the equatorial Pacific amplifies
79 local convection, causing an increase in convective clouds. Consequently, incoming short-
80 wave radiation is attenuated, leading to a decrease in the initial SST warming and the
81 local convection. The restrained convection subsequently diminishes the intensity and
82 the westward extension of the WNPSH. However, it is challenging to disentangle the rel-
83 ative impact of the tropical SST and precipitation on the inter-model spread of the NPSH
84 projections in a coupled atmosphere-ocean system, given the complexity of their rela-
85 tionship (e.g., Xie et al. (2010b); P. Huang et al. (2013); J. He et al. (2014)). As a re-
86 sult, how model variability in tropical precipitation, both driven by inter-model SST spread
87 and otherwise, influences the NPSH remains largely unexplored. Furthermore, the im-
88 pacts of diabatic heating on subtropical highs have been examined primarily through ide-
89 alized baroclinic wave models with a simplified atmosphere (Ting et al., 2001; Rodwell
90 & Hoskins, 2001; Duan et al., 2017; Park & Lee, 2021). Therefore, the potential influ-
91 ences of diabatic heating on other factors such as land surface temperature (TS), which
92 could potentially modulate the NPSH, have yet to be explored.

93 In this study, we utilize output from the coupled and atmosphere-only simulations
94 from the Coupled Model Intercomparison Project (CMIP and AMIP) to identify the lead-
95 ing modes of inter-model spread in summer NPSH projections. We further explore the
96 mechanisms underlying such uncertainties by prescribing diabatic heating in a compre-
97 hensive atmospheric general circulation model (AGCM) and a simple baroclinic station-
98 ary wave model. The relative roles of model differences in tropical precipitation inde-
99 pendent of tropical inter-model SST spread and tropical precipitation driven by trop-
100 ical inter-model SST spread are explored in detail. The connection between the inter-
101 model spread of the NPSH projections and inter-model spread of extra-tropical land TS
102 projections is also discussed.

103 2 Data and Method

104 2.1 CMIP and AMIP data

105 We use monthly mean data from fully coupled Abrupt4×CO₂ and pre-industrial
106 control simulations of 46 models (Table S1) from both CMIP5 and CMIP6 (Taylor et
107 al., 2012; O’Neill et al., 2016). Only one ensemble member (r1i1p1 or r1i1p1f1) is selected
108 from each model. All data are interpolated to horizontal grids with 1°×1° spacing and
109 17 pressure levels. To investigate the inter-model uncertainties that are independent of
110 inter-model differences in SST changes, we analyze 15 AMIP models (Table S1) from both
111 CMIP5 and CMIP6. Three AMIP scenarios are considered: (1) AMIPControl, the con-
112 trol simulation forced by observational monthly mean SST and sea ice concentration; (2)
113 AMIP4×CO₂, same as AMIPControl but with CO₂ concentration quadrupled; (3) AMIP-

114 Future, same as AMIPControl except adding the SST anomaly pattern taken from CMIP3
 115 experiments at the time of CO_2 quadrupling but adjusted to achieve a global mean warm-
 116 ing of 4K in SST (Webb et al., 2017). The response (Δ) is calculated as the difference
 117 between forced and control simulation. We take the last 30-year June to August mean
 118 (JJAm) from the 150-year Abrupt4x CO_2 , and 30-year JJAm from AMIPFuture and AMIP4x CO_2
 119 as equilibrium responses. For each coupled model under the Abrupt4x CO_2 scenario,
 120 we first compute its equilibrium global mean SST (ΔSST_{gm}) response, and subsequently
 121 adjust the response of other variables by the ratio $\frac{4}{\Delta SST_{gm}}$, assuming that these variables
 122 respond proportionally to changes in global mean SST. The multi-model ensemble mean
 123 (MMM) equilibrium response of Abrupt4x CO_2 is approximately equal to the summa-
 124 tion of AMIP4x CO_2 and AMIPFuture (AMIP4x CO_2 +Future) (Figure S1 and S2; J. He
 125 and Soden (2015); Chadwick et al. (2017)).

126 We use eddy streamfunction at 850 hPa to represent the NPSH (Ψ_{850}) (Wills et
 127 al., 2019; Shaw & Voigt, 2015). Because diabatic heating is not a standard output from
 128 CMIP/AMIP, it was calculated as a residual from the time-mean thermodynamic en-
 129 ergy equation (Rodwell & Hoskins, 2001):

$$\frac{\bar{Q}}{c_p} = \frac{\partial \bar{T}}{\partial t} + \left(\frac{p}{p_0}\right)^{\frac{R}{c_p}} \bar{\omega} \frac{\partial \bar{\theta}}{\partial p} + \bar{\mathbf{v}} \cdot \nabla_{\mathbf{p}} \bar{T} + \left(\frac{p}{p_0}\right)^{\frac{R}{c_p}} \frac{\partial}{\partial p} (\bar{\omega}' \theta') + \nabla_{\mathbf{p}} \cdot (\bar{\mathbf{v}}' T') \quad (1)$$

130
 131
 132 where Q is the diabatic heating or cooling, T is the temperature, c_p is the specific heat
 133 of dry air at constant pressure, R is the gas constant for dry air, p is the pressure, θ is
 134 the potential temperature, ω is the pressure velocity, and \mathbf{v} are the horizontal wind ve-
 135 locities. The overbar represents the climatological June to August mean and prime is
 136 the deviation from that mean. Since monthly data is employed to calculate Eq. 2.1, the
 137 resultant diabatic heating also includes the temperature tendency due to heat transport
 138 by sub-monthly transients. Over the tropical ocean, the pattern of vertically integrated
 139 diabatic heating resembles the pattern of precipitation as the diabatic heating is domi-
 140 nated by condensational heating (Hagos et al., 2010).

141 2.2 Inter-model Uncertainty Analysis

142 We refer to the inter-model uncertainty (or spread) as the deviation of the equi-
 143 librium response of each individual model from the MMM (Figure S3 and S4). The re-
 144 gions with large inter-model spread were first identified via inter-model standard devi-
 145 ations (Figure 1a). The leading modes of inter-model variability are further analyzed by
 146 the rotated inter-model empirical orthogonal function with varimax criterion (IEOF) (Fig-
 147 ure 1b to 1d):

$$\delta \Delta X(m, s) = \sum_{i=1}^n IPC_{m,i} \cdot IEOF_{i,s} \quad (2)$$

149 where ΔX denotes the projected changes of variable X (e.g., Ψ_{850} , precipitation), δ is
 150 the deviation from the MMM, s is the number of spatial grid points, m is the number
 151 of models, and n is the number of modes. The principal components (IPCs) are normal-
 152 ized. We opted for rotated IEOF over un-rotated IEOF to optimize the inter-model vari-
 153 ance captured within the same modes, thus enhancing their physical interpretability. (Mestas-
 154 Nuñez, 2000). To quantify the connection between the spread in two variables (e.g., X
 155 and Y), we calculate the relationship between the inter-model variability in Y and the
 156 i th mode of IEOF of variable X , through two approaches: (1) by regressing Y onto the
 157 corresponding i th inter-model principal component (IPC_i) of X , or (2) by selecting where
 158 IPC_i values of X are statistically significant, i.e., exceeding one standard deviation, and

159 compositing Y using models with significant positive IPC_i values and models with sig-
 160 nificant negative IPC_i values .

161 With a limited number of models, the inter-model spread may be more sensitive
 162 to specific outliers. Therefore, we analyzed the inter-model standard deviations of $\Delta NPSH$
 163 within a subset of 15 CMIP models for which the corresponding AMIP outputs are avail-
 164 able (Figure S5a; Table S1). The similarity between Figure 1a and Figures S5a suggests
 165 that this subset of 15 models is sufficient to capture the spatial structures of $\Delta NPSH$
 166 inter-model spread found in the larger ensemble.

167 2.3 Model Simulations

168 To investigate the physical mechanisms underlying the inter-model uncertainty of
 169 $\Delta NPSH$, we use both the Community Atmosphere Model, version 5 (CAM5) within the
 170 framework of the Community Earth System Model, version 1 (CESM1) (Hurrell et al.,
 171 2013), and a baroclinic stationary wave model (SWmodel) (Ting & Yu, 1998; Held et
 172 al., 2002) to perform the sensitivity experiments. A comprehensive description of both
 173 models is provided in Table S2. Both CAM5 and the SWmodel are adequate for sim-
 174 ulating the response of large-scale atmospheric circulation to prescribed forcing. How-
 175 ever, CAM5 is more representative of the real atmosphere as it incorporates a much wider
 176 range of processes and is not subject to the relaxation toward a basic state or the ide-
 177 alized dampings that the SWmodel is. Specifically with CAM5, we are able to explore
 178 the associated response of land surface temperature, cloud cover and precipitation to pre-
 179 scribed forcing. In contrast, the SWmodel only focuses on the atmospheric stationary
 180 wave response which helps us to understand the dynamics and interactions of waves with-
 181 out confounding effects of other climate feedbacks, but it is an idealized model in which
 182 interactions, such as eddy-feedbacks, must be prescribed, and it is kept stable through
 183 relaxation toward a specified basic state and the addition of idealized damping. The con-
 184 trol simulation in CAM5 was forced with the climatological SSTs and sea ice concentra-
 185 tions taken from the pre-industrial simulation of the CESM1 Large Ensemble Project
 186 (LENS) (Kay et al., 2015). The basic state in the SWmodel is the three-dimensional bo-
 187 real summer climatology including temperature and horizontal winds, derived from the
 188 same LENS pre-industrial simulation mentioned above. Note that the orography forc-
 189 ing is integrated into the 3D climatological basic state in SWmodel.

190 We explore the tropical influence on the NPSH via a series of diabatic heating sen-
 191 sitivity experiments. Specifically, we consider two types of inter-model spreads of the trop-
 192 ical diabatic heating ($\delta\Delta Q$): one that is independent of inter-model spread in tropical
 193 SST change ($\delta\Delta SST$) and the other that is induced by the tropical $\delta\Delta SST$. The $\delta\Delta SST$ -
 194 independent $\delta\Delta Q$ is derived from the rotated IEOF analysis on AMIP4 \times CO₂+Future
 195 models over the entire tropics (30°S-30°N), where SST and changes in SST are the same
 196 among models. The pattern of vertically integrated diabatic heating resembles Figure
 197 2c. To quantify $\delta\Delta Q$ attributed to tropical $\delta\Delta SST$, we begin by imposing the tropical
 198 $\delta\Delta SST$ associated with $\delta\Delta NPSH$ on CAM5 control simulation. The SST anomalies are
 199 determined through the rotated IEOF analysis of the output from the CMIP Abrupt4 \times CO₂
 200 experiment (“Data and Method 2.2”, Figure 2d). The resulting total diabatic heating
 201 anomaly (Figure S7a) over the deep tropics (15°S-15°N) is then calculated as the sum
 202 of condensational heating, longwave heating, solar heating and vertical diffusion of tem-
 203 perature. The diabatic heating anomaly is added to the SWmodel as a constant tem-
 204 perature tendency term. For each SWmodel experiment, the model is integrated for 50
 205 days, and the time average of the last 20 days is taken as the equilibrium response. Since
 206 CAM5 would non-linearly amplify the diabatic heating perturbation due to its moisture
 207 process and other feedbacks, we determine the diabatic heating perturbation to impose
 208 with an “iterative approach” as detailed in R. Chen et al. (2022). For each CAM5 ex-
 209 periment, five ensembles of three-month simulations are branched off on the first day of

210 June of different years. The equilibrium responses are calculated as the three-month mean
 211 of the differences between the forced and control runs averaged across all ensembles.

212 To compare the relative importance of inter-model spread in extra-tropical SST changes
 213 to the tropical influence, we prescribe the $\delta\Delta\text{SST}$ associated with inter-model spread of
 214 ΔNPSH over the North Pacific ($27 - 70^\circ\text{N}$) to CAM5. The North Pacific SST inter-
 215 model spread is calculated through inter-model composite analysis from Abrupt4xCO₂
 216 output (“Data and Method 2.2”, Figure S6).

217 3 Results

218 3.1 Overview of Inter-model Spread in Summer NPSH Projection

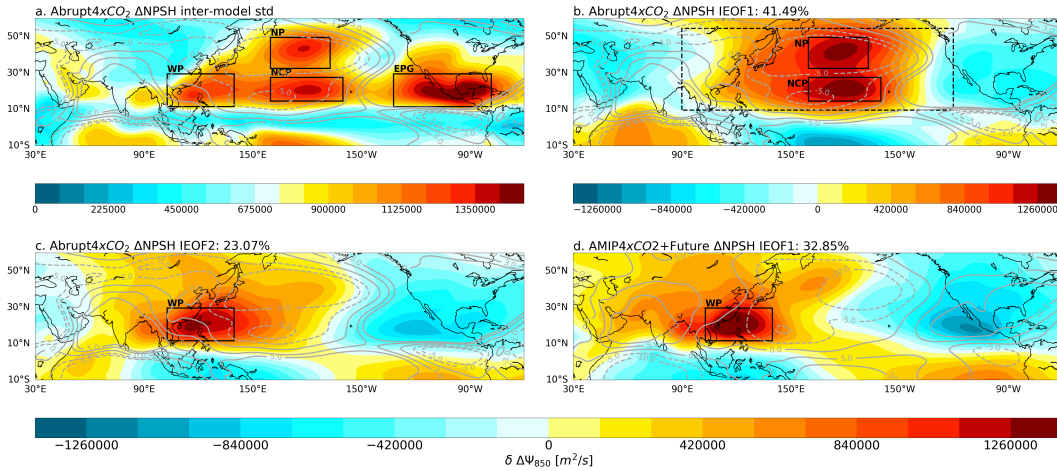


Figure 1. Inter-model spread of summer NPSH future projections. **a** The inter-model standard deviation of $\Delta\Psi_{850}$ under the Abrupt4xCO₂ experiment. Four regions with high inter-model variability are marked with black rectangles. **b,c** The first two leading modes (IEOF1 and IEOF2) derived from IEOF analysis on $\Delta\Psi_{850}$ over the domain ($10-50^\circ\text{N}, 90-240^\circ\text{E}$; regions outlined with dashed line in **b**) under Abrupt4xCO₂ experiment. **d** Same as **b** but for AMIP4xCO₂+Future experiment. The grey contours denote the ΔNPSH MMM (unit: $10^6\text{m}^2\text{s}^{-1}$) under Abrupt4xCO₂ (**a** to **c**) and AMIP4xCO₂+Future (**d**), respectively. The percentage of inter-model variance explained by each mode is included in the subtitle.

219 The overall strength of summer NPSH weakens under the Abrupt4xCO₂ scenario
 220 as indicated by the MMM response of Ψ_{850} (grey contours in Figure 1a) across 46 CMIP
 221 models. However, the inter-model standard deviation of ΔNPSH is comparable or even
 222 larger than the MMM response in most of the regions (compare color shadings and con-
 223 tours in Figure 1a). We find four zones of high ΔNPSH inter-model variability: the west-
 224 ern Pacific (WP), the eastern Pacific and Gulf of Mexico (EPG), the North Pacific (NP)
 225 and the central North Pacific (NCP). These four hot spots are well captured by the first
 226 two leading IEOF modes which account for nearly 65% of the inter-model variance (Fig-
 227 ure 1b and 1c). Here we pick the sign of the eigenvectors that features a strengthening
 228 of the NPSH as the positive direction and all subsequent analyses follow this choice. The
 229 shape of the IEOF patterns, the amount of inter-model variance explained, and the un-
 230 derlying physical mechanisms remain the same regardless of our choice (Weare et al., 1976).
 231 The first IEOF features an overall strengthening of the NPSH with two centers of max-
 232 imum variance located at the NP and the NCP respectively. The cyclones over the Asian

233 continent and the EPG are also partially captured (Figure 1b). The second IEOF mode
 234 presents a dipole structure representing a strengthening and westward extension of the
 235 WNPSH, and a weakening of the NPSH over the eastern Pacific (Figure 1c). Mechanisms
 236 behind the two IEOF modes will be examined in the rest of the paper.

237 To exclude the influence from inter-model variability in SST changes, we evaluate
 238 the inter-model spread of the NPSH response among 15 models under AMIP4×CO₂+Future,
 239 where all models are driven by the same SST changes (“Data and Method 2.1” and Table
 240 S1). Note that these 15 models are also included in the coupled Abrupt4×CO₂ experiments
 241 and can capture the overall spatial patterns of ΔNPSH inter-model spread (Figure
 242 S8). As depicted in Figure S5b, the WP region demonstrates a notable inter-model
 243 standard deviation among 15 AMIP4×CO₂+Future models. The leading inter-model
 244 variance pattern (Figure 1d) features a dipole structure with an anticyclone anomaly over
 245 the WP that resembles Figure 1c, suggesting that the inter-model spread of ΔWNPSH
 246 over the WP has causes not related to δΔSST. We’ve additionally examined the δΔSST
 247 associated with the IEOF2 of ΔNPSH under Abrupt4×CO₂. As shown in Figure S9,
 248 the IPC2 of ΔNPSH does not significantly correlate to ΔSST in most of the regions (Figure
 249 S9b). On the other hand, the high inter-model variances over the NP and NCP (Figure
 250 1b) are either absent or underrepresented in Figure 1d and Figure S5b, indicating
 251 that the inter-model uncertainties of ΔNPSH over the NP and the NCP might be related
 252 to ΔSST inter-model spread.

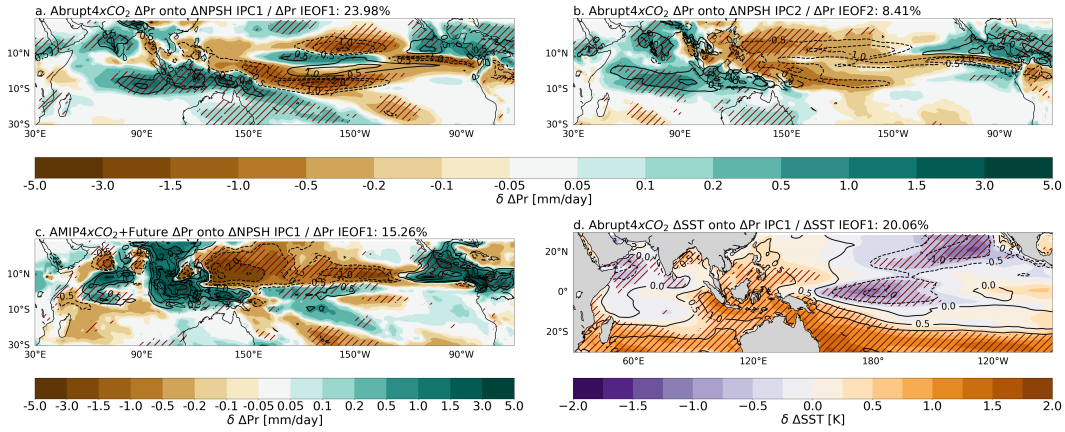


Figure 2. Tropical precipitation (Pr) and SST anomalies associated with ΔNPSH inter-model spread. **a** Tropical ΔPr regressed onto IPC1 of ΔNPSH (shadings) and IEOF1 of ΔPr (contours; mm/day) under Abrupt4xCO₂ scenario. **b** Similar to **a** but with ΔPr regressed onto IPC2 of ΔNPSH and IEOF2 of ΔPr. **c** Similar to **a** and **b** but with ΔPr regressed onto IPC1 of ΔNPSH and IEOF1 of ΔPr under AMIP4xCO₂+Future. **d** Tropical ΔSST regressed onto IPC1 or ΔPr (shadings) and IEOF1 of ΔSST (contours; K). Regions with statistically significant correlations are hatched.

253 3.2 Tropical Origins of the Inter-model Uncertainty

254 As a key driver of the tropical circulation and the tropical-extratropical telecon-
 255 nections, (Gill, 1980; Emanuel et al., 1994; Fereday et al., 2020), the tropical precipita-
 256 tion (Pr) remains one of the most challenging components in climate projections. We
 257 examined the inter-model variability in the equilibrium response of tropical precipita-
 258 tion under the Abrupt4×CO₂ scenarios via the rotated IEOF method and evaluate their
 259 relationships with ΔNPSH. The IEOF1 of the tropical precipitation response displays

a meridional alternating negative and positive anomaly structure spanning from the Indian Ocean to the subtropical Pacific (contours in Figure 2a). The second leading mode of the precipitation inter-model spread exhibits a southwest-northeast orientated dipole pattern with negative convection anomalies located in the west Pacific (contours in Figure 2b). The first two leading IEOF modes account for around 32% of the inter-model variance of the tropical precipitation response. When regressing the precipitation response onto the inter-model IPCs of Δ NPSH, we find the regression pattern associated with IEOF1 of Δ NPSH aligns closely with the corresponding IEOF1 of tropical Δ Pr, while the regression pattern associated with IEOF2 of Δ NPSH aligns closely with the corresponding IEOF2 of tropical Δ Pr (comparing shadings to contours in Figure 2a and 2b).

3.2.1 Contribution of $\delta\Delta$ SST Independent Precipitation Uncertainty

Given the resemblance between Figure 1c and 1d, and the significant correlation between tropical precipitation and the NPSH, as suggested in Figure 2b, we initiated our investigation by focusing on non- $\delta\Delta$ SST related precipitation inter-model spread. Under AMIP4 \times CO₂+Future (Figure 2c), the spatial pattern of IEOF1 of tropical precipitation response also exhibits a dipole pattern oriented from southwest to northeast over the Indo-West Pacific similar to Figure 2b. This precipitation dipole is related to an asymmetric diabatic heating with respect to the equator and this diabatic heating pattern will trigger a low-level anticyclone (cyclone) to the north (south) of the equator, as described by the Matsuno-Gill response (Gill, 1980; Matsuno, 1966). Indeed, the low-level anticyclone at the WP, and the cyclone at the Maritime Continent (MC) in Figure 1c and 1d appear to align with the Matsuno-Gill response to the Indo-West Pacific precipitation dipole anomalies demonstrated in Figures 2b and 2c. This consistency led us to hypothesize that the high $\delta\Delta$ NPSH in the WP region can be triggered and sustained by $\delta\Delta$ Q that is independent of tropical $\delta\Delta$ SST.

To confirm our hypothesis, we conducted a set of sensitivity experiments in CAM5 and the SWmodel where the tropical (30°S–30°N) inter-model diabatic heating anomaly obtained from the AMIP4 \times CO₂+Future output is prescribed (“Data and Method 2.3”). As demonstrated in Figure 3e and 3g, a quadrupole low-level circulation pattern with a strong anticyclone centered at the WP and a strong cyclone centered at the EPG appears as a primary response to the tropical diabatic heating. In the case of CAM5, the anomalous northeasterlies on the eastern flank of the anticyclone transport the off-equatorial dry (low moist enthalpy) air into the western Pacific, further suppressing the convection over the WP (Wu et al., 2017; Y. Wang et al., 2022). Moreover, the elevated land surface temperature over the extra-tropical Eurasian continent (Figure 4c) acts to reinforce the strengthening of the NPSH through the land-sea thermal contrast (Portal et al., 2022; Shaw & Voigt, 2015). The similar response of $\Delta\Psi_{850}$ between CAM5 (Figure 3e) and the SWmodel (Figure 3g) suggests that the strengthening of the NPSH over the WP can be primarily attributed to the Matsuno-Gill response triggered by tropical $\delta\Delta$ Q. Besides the Matsuno-Gill response, the summer mean state of the Indo-West Pacific climate establishes a niche environment to sustain the low-level circulation anomalies over the WP region. This is achieved through the positive barotropic kinetic energy conversion from the climatological confluence between the monsoon westerlies and trade winds at low levels (Hoskins et al., 1983; X. Wang et al., 2021). The upper-level circulation presents a similar quadrupole pattern but with a cyclone over the western Pacific and anticyclone over North America and the EPG, suggesting a baroclinic wave structure between 15–20°N (Figure 3a and 3c) (Wills et al., 2019; Ting & Yu, 1998). As shown by the Takaya-Nakamura wave activity flux (Figure 3a), a northeastward propagating Rossby wave train emanates from the tropical western Pacific and extends to North America over the upper troposphere (Ding et al., 2018; Takaya & Nakamura, 1997). The upper-level eddy streamfunction response to non- $\delta\Delta$ SST induced $\delta\Delta$ Q, simulated by both CAM5 and the SWmodel, generally aligns with the statistical results derived from the IEOF analysis (Figure S10c and S10d). In SWmodel, the weaker response of barotropic structure above

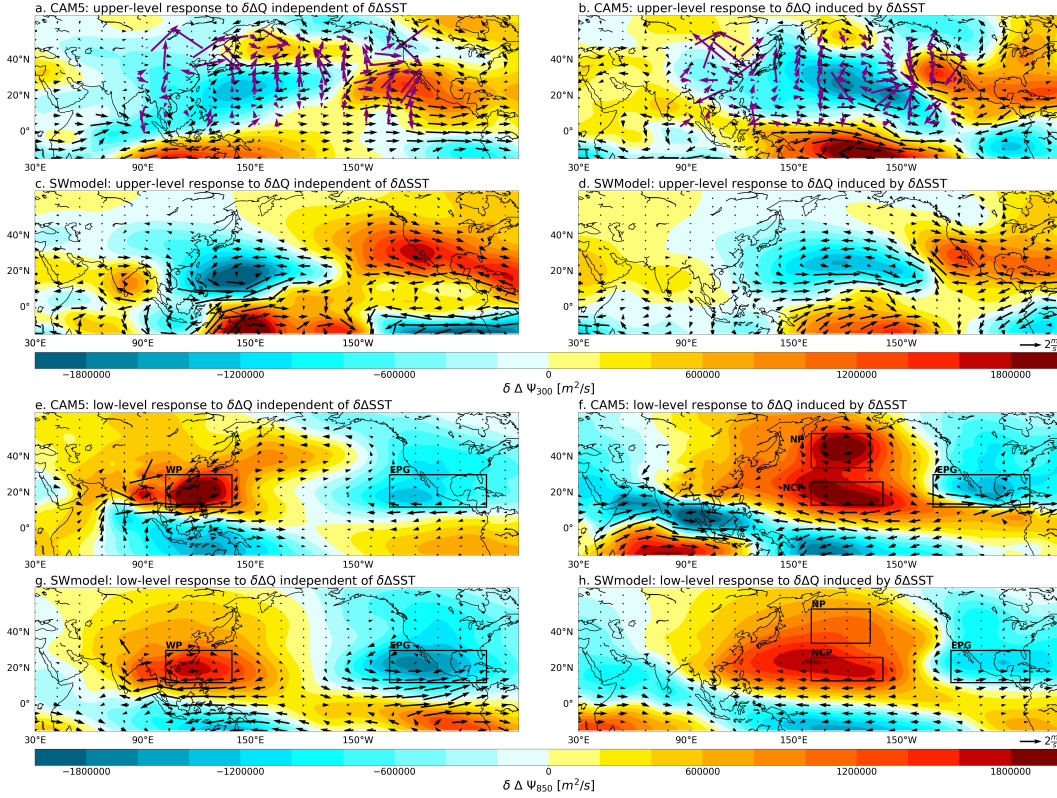


Figure 3. Response of subtropical circulation to prescribed tropical diabatic heating anomalies ($\delta\Delta Q$) in CAM5 and SWmodel. The left column shows the response of eddy streamfunction (shadings) and horizontal winds (black vectors; m/s) to $\delta\Delta Q$ independent of tropical ΔSST inter-model spread ($\delta\Delta SST$). The right column is similar to the left one but with the circulation response to tropical $\delta\Delta SST$ induced $\delta\Delta Q$. **a-d** describe the results at 300 hPa and **e-h** describe the results at 850 hPa. The stationary Rossby wave propagation is shown as the Takaya-Nakamura Flux (purple vectors; normalized) in **a** and **b**. The CAM5 results are **a**, **b**, **e** and **f** and the SWmodel results are **c**, **d**, **g** and **h**.

313 40° N and the lack of low-level anticyclonic anomaly over the southwest of the Bering
 314 Sea, when compared to CAM5, could be attributed to the simplicity of the model
 315 and the absence of features such as anomalies in the transient eddies or extra-tropical dia-
 316 batic processes (Figure S11), and non-linear interactions of the anomalies with topog-
 317 raphy.

3.2.2 Contribution of $\delta\Delta SST$ -driven Precipitation Uncertainty

319 The interaction between tropical SST and subtropical atmospheric circulation is
 320 often discussed in the context of the El Niño-Southern Oscillation teleconnection, such
 321 as the Pacific-North American pattern (e.g., Franzke et al. (2011); Dai et al. (2017)), Kelvin
 322 wave-induced Ekman divergence resulting from Indian Ocean (IO) warming (C. He &
 323 Zhou, 2014; Xie et al., 2009), local convection over a warm MC (Sui et al., 2007), moist
 324 enthalpy advection (Wu et al., 2017), and the ocean-atmosphere coupling between the
 325 IO SST and the Pacific-Japan pattern (Kosaka et al., 2013). In particular, by modify-
 326 ing the local convection, tropical SST can modulate the influence of tropical precipita-
 327 tion on atmospheric circulation via wave generation and propagation. Therefore, it is

328 plausible to speculate that the inter-model spread of tropical SST affects the NPSH by
 329 generating anomalous tropical precipitation. The IEOF1 of tropical Δ SST features a La
 330 Niña-like pattern with cooling over the western Indian Ocean and central Pacific and a
 331 K-shaped warming anomaly covering the MC and the western subtropical Pacific (Fig-
 332 ure 2d and Figure S9a). This SST inter-model spread pattern is spatially correlated with
 333 the IEOF1 of precipitation (comparing contours to shadings in Figure 2d). In the mean-
 334 time, the tropical precipitation anomaly regressed onto IPC1 of Δ NPSH (shadings in Fig-
 335 ure 2b) perfectly lines up with the IEOF1 pattern of precipitation, implying that the high
 336 inter-model Δ NPSH variance at the NP and the NCP are connected to the tropical pre-
 337 cipitation anomalies that are linked to the inter-model Δ SST uncertainty.

338 The role of the tropical $\delta\Delta$ SST-driven precipitation inter-model spread is further
 339 explored through numerical experiments (“Data and Method 2.3”). To focus on the im-
 340 pact of inter-model precipitation uncertainty in the deep tropics, we only prescribe di-
 341 abatic heating anomalies between $15^{\circ}S$ - $15^{\circ}N$ generated from the tropical $\delta\Delta$ SST exper-
 342 iment to CAM5 and the SWmodel. As shown in both Figure 3f and Figure 3h, a Matsuno-
 343 Gill type circulation response appears in the lower troposphere in both CAM5 and the
 344 SWmodel. However, the two high-pressure centers located at the NP and the NCP are
 345 only captured by CAM5. The IEOF1 pattern of Δ NPSH (Figure 1b) is well replicated
 346 in CAM5 except that the anomaly over the NCP is inclined towards the northwest. The
 347 NPSH response in the SWmodel displays only one high-pressure center located around
 348 NCP and this could result from neglecting other extra-tropical process such as transient
 349 eddy feedbacks (Figure S12). The circulation response in the upper troposphere in both
 350 CAM5 and the SWmodel exhibits a northeastward propagating Rossby wave train, a baro-
 351 clinic wave structure between 15 - $20^{\circ}N$ and a barotropic wave structure between 45 - $55^{\circ}N$
 352 (Figure 3b, Figure 3d and Figure S10b). It is worth mentioning that the influence of the
 353 tropical inter-model Δ SST spread extends beyond local convection to include precipi-
 354 tation changes in remote areas (contours in Figure S7b). The secondary convection pro-
 355 duced over the extra-tropics also exerts an impact on the NPSH along with the tropi-
 356 cal convection. For instance, the positive precipitation anomaly over East China Sea trig-
 357 gers a local cyclonic circulation anomaly, restricting the westward extension of the $\delta\Delta$ NPSH
 358 (shadings in Figure S7b).

359 3.3 Relationship with the Extra-tropics

360 While we have determined that the primary sources of model uncertainty in Δ NPSH
 361 are related to both $\delta\Delta$ SST and non- $\delta\Delta$ SST driven tropical precipitation inter-model spread,
 362 it is also important to consider the potential connections to extra-tropical SST and land
 363 TS. As illustrated in Figure 4a, the inter-model spread of land TS changes features an
 364 overall warming in northern Eurasia between 45 - $65^{\circ}N$ and a cooling in South Asia and
 365 the Middle East. The high inter-model variability of Δ NPSH over the WP is statisti-
 366 cally associated with this warming pattern over extra-tropical Eurasia, while the other
 367 three hot spots do not exhibit any significant correlations (shadings in Figure 4a , Fig-
 368 ure S13 and S14). When examining the inter-model spread of extra-tropical land TS re-
 369 sponse under the AMIP4x CO_2 +Future, we find a similar warming pattern between 45 -
 370 $65^{\circ}N$ and this pattern is also significantly correlated with IPC1 of Δ NPSH (Figure 4b).

371 The conventional perspective believes that the strengthening of the NPSH is mostly
 372 driven by an enhanced land-sea thermal contrast (Li et al., 2012; Shaw & Voigt, 2015;
 373 Levine & Boos, 2019; Wills et al., 2019; Portal et al., 2022). In addition to that, we find
 374 that a substantial portion of the inter-model spread of extra-tropical land warming over
 375 northern Eurasia (Figure 4a and 4b) can also be produced by prescribing CAM5 with
 376 non- $\delta\Delta$ SST driven diabatic heating anomalies (shadings in Figure 4c). The westward
 377 extension of the anomalous low-level anticyclone induced by the tropical diabatic heat-
 378 ing inter-model spread is evident over Eurasia (Figure 3e and 3g). This extension inten-
 379 sifies the subsidence of dry air and leads to a reduction in cloud fractions, particularly

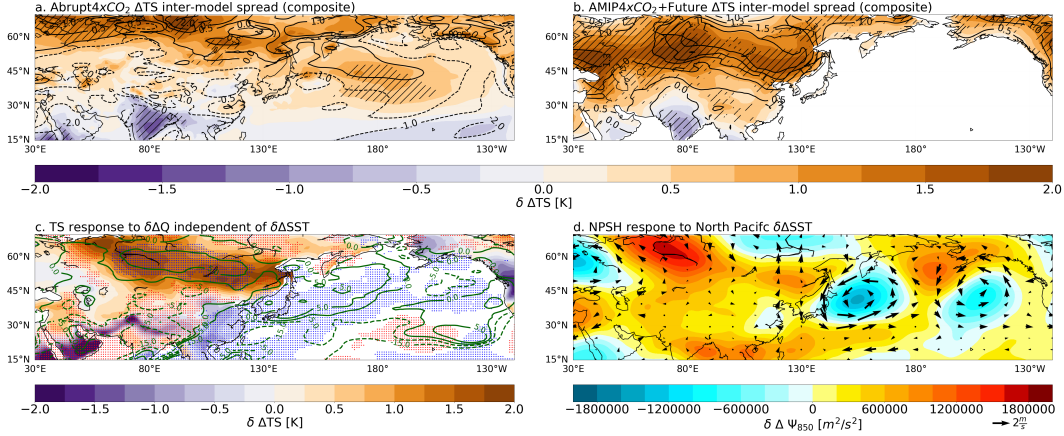


Figure 4. Relationship between inter-model uncertainty of Δ NPSH and extra-tropical land Δ TS and the North Pacific Δ SST. **a** Extra-tropical Δ TS regressed onto IPC2 of Δ NPSH (shadings) and inter-model uncertainty of Δ TS from composite analysis (contours; K). **b** Similar to **a** but with land Δ TS regressed onto IPC1 of Δ NPSH and Δ TS inter-model uncertainty under the AMIP4xCO₂+Future. Regions with statistically significant correlations are marked with hatches in **a** and **b**. **c** Response of land TS (shadings; K), net surface shortwave radiation (thick green contours; W/m^2), and low cloud fraction (scatters in blue and red, where blue indicates a significant low cloud reduction and vice versa) to SST independent inter-model tropical diabatic heating spread in CAM5. **d** Response of NPSH (shadings) and horizontal winds (vectors; m/s) to North Pacific $\delta\Delta$ SST.

380 for low clouds (blue scatters in Figure 4c). The reduction of the low clouds further pro-
 381 motes the absorption of solar radiation by the land, leading to a net increase of the down-
 382 welling shortwave radiation at the land surface (thick green contours in Figure 4c). In
 383 addition, the anomalous low-level southerly winds contribute to the extra-tropical land
 384 warming by advecting warmer air from the tropics (Figure 3e and 3g). On the other hand,
 385 the extra-tropical Eurasian warming is also expected to reinforce the intensification of
 386 the $\delta\Delta$ NPSH.

387 By regressing the inter-model Δ SST anomalies over the North Pacific onto the IPC2
 388 of Δ NPSH, we find a warm anomaly stretching from the Kuroshio Extension to the west
 389 coast of Canada (Figure 4a). This warm SST anomaly along the Kuroshio Extension is
 390 also correlated with an enhancement of local precipitation and a reduction of precipi-
 391 tation to the north and south (Figure S15a) (Gan & Wu, 2012). When prescribing the
 392 $\delta\Delta$ SST over the North Pacific to CAM5 (“Data and Method 2.3”), a very weak strength-
 393 ening of the low-level circulation is seen over the NP, and two cyclonic circulations are
 394 shown in the western and eastern North Pacific as local responses to the enhancement
 395 of precipitation (Figure S15b). Nevertheless, the overall structure of the NPSH response
 396 is quite different from IEOFs of Δ NPSH (Figure 1). Conversely, the strengthening of the
 397 NPSH triggered by tropical precipitation inter-model spread leads to an overall reduc-
 398 tion of low cloud fraction and intensification of downwelling surface shortwave radiation,
 399 which could partially explain the warming over the North Pacific (Figure 4c).

400 4 Summary and Discussion

401 We have confirmed that the model uncertainties in projections of the NPSH origi-
 402 nate from both $\delta\Delta$ SST and non- $\delta\Delta$ SST driven tropical inter-model precipitation spread.

Specifically, the large model variance of Δ NPSH over the WP is caused by inter-model precipitation uncertainty that is independent of $\delta\Delta$ SST. This inter-model Δ NPSH spread further influences changes in extra-tropical Eurasian TS and the North Pacific SST through the modulation of low cloud fraction. On the other hand, the inter-model spread in the changes of tropical SST can affect the NPSH over the NP and the NCP through the production of anomalous precipitation.

Our study highlights the importance of accurately projecting the tropical precipitation. When the model variance is absent in Δ SST, the two plausible causes of inter-model precipitation spread could be models' diversity in cloud parameterization (Su et al., 2017; Mauritsen & Stevens, 2015) and tropical land albedo simulation (Levine & Boos, 2017; W. Zhou & Xie, 2017). In addition, other processes such as the subtropical transient eddy feedback (e.g., Hurrell et al. (2013)), the subtropical and mid-latitude cloud albedo feedback (Burls et al., 2017), and the Arctic amplification (e.g., Coumou et al. (2018)) might also contribute to the model uncertainty in projections of the NPSH and are worth deeper explorations.

Open Research Section

The CMIP5 data can be downloaded publicly at: CMIP5 (2012) (or <https://esgf-node.llnl.gov/projects/cmip5/>), and the CMIP6 data can be downloaded publicly at: CMIP6 (2016) (or <https://esgf-node.llnl.gov/projects/cmip6/>). The numerical experiment data of this paper are archived at Zenodo. (Lu et al., 2023)

Acknowledgments

We thank the two anonymous reviewers for their valuable and insightful comments. We also thank the computational resources provided by the Partnership for an Advanced Computing Environment (PACE) at Georgia Institute of Technology, and the Cheyenne supercomputer provided by the Computational and Information Systems Laboratory at the National Center for Atmospheric Research. KL and JH are supported by the National Science Foundation AGS-2047270. IRS is supported by the National Center for Atmospheric Research, which is a major facility sponsored by the National Science Foundation under the Cooperative Agreement 1852977.

References

- Baker, H. S., Woollings, T., Mbengue, C., Allen, M. R., O'Reilly, C. H., Shiogama, H., & Sparrow, S. (2019). Forced summer stationary waves: the opposing effects of direct radiative forcing and sea surface warming. *Climate Dynamics*, *53*(7), 4291–4309. Retrieved from <https://doi.org/10.1007/s00382-019-04786-1> doi: 10.1007/s00382-019-04786-1
- Boos, W. R., & Hurley, J. V. (2013). Thermodynamic bias in the multimodel mean boreal summer monsoon. *Journal of Climate*, *26*(7), 2279–2287. Retrieved from <https://journals.ametsoc.org/view/journals/clim/26/7/jcli-d-12-00493.1.xml> doi: <https://doi.org/10.1175/JCLI-D-12-00493.1>
- Burls, N. J., Muir, L., Vincent, E. M., & Fedorov, A. (2017). Extra-tropical origin of equatorial pacific cold bias in climate models with links to cloud albedo. *Climate Dynamics*, *49*(5), 2093–2113. Retrieved from <https://doi.org/10.1007/s00382-016-3435-6> doi: 10.1007/s00382-016-3435-6
- Chadwick, R., Douville, H., & Skinner, C. B. (2017). Timeslice experiments for understanding regional climate projections: applications to the tropical hydrological cycle and european winter circulation. *Climate Dynamics*, *49*(9), 3011–3029. Retrieved from <https://doi.org/10.1007/s00382-016-3488-6> doi: 10.1007/s00382-016-3488-6

- 451 Chen, M., Yu, J.-Y., Wang, X., & Jiang, W. (2019, 2023/03/03). The chang-
 452 ing impact mechanisms of a diverse el niño on the western pacific subtrop-
 453 ical high. *Geophysical Research Letters*, *46*(2), 953–962. Retrieved from
 454 <https://doi.org/10.1029/2018GL081131> doi: [https://doi.org/10.1029/](https://doi.org/10.1029/2018GL081131)
 455 [2018GL081131](https://doi.org/10.1029/2018GL081131)
- 456 Chen, R., Simpson, I. R., Deser, C., Wang, B., & Du, Y. (2022). Mechanisms be-
 457 hind the springtime north pacific enso teleconnection bias in climate mod-
 458 els. *Journal of Climate*, *35*(23), 4091–4110. Retrieved from [https://](https://journals.ametsoc.org/view/journals/clim/35/23/JCLI-D-22-0304.1.xml)
 459 journals.ametsoc.org/view/journals/clim/35/23/JCLI-D-22-0304.1.xml
 460 doi: <https://doi.org/10.1175/JCLI-D-22-0304.1>
- 461 Chen, X., Zhou, T., Wu, P., Guo, Z., & Wang, M. (2020). Emergent constraints on
 462 future projections of the western north pacific subtropical high. *Nature Com-*
 463 *munications*, *11*(1), 2802. Retrieved from [https://doi.org/10.1038/s41467-](https://doi.org/10.1038/s41467-020-16631-9)
 464 [-020-16631-9](https://doi.org/10.1038/s41467-020-16631-9) doi: [10.1038/s41467-020-16631-9](https://doi.org/10.1038/s41467-020-16631-9)
- 465 Choi, J., Lu, J., Son, S.-W., Frierson, D. M. W., & Yoon, J.-H. (2016, 2023/03/03).
 466 Uncertainty in future projections of the north pacific subtropical high and its
 467 implication for california winter precipitation change. *Journal of Geophysical*
 468 *Research: Atmospheres*, *121*(2), 795–806. Retrieved from [https://doi.org/](https://doi.org/10.1002/2015JD023858)
 469 [10.1002/2015JD023858](https://doi.org/10.1002/2015JD023858) doi: <https://doi.org/10.1002/2015JD023858>
- 470 Choi, W., & Kim, K.-Y. (2019). Summertime variability of the western north pa-
 471 cific subtropical high and its synoptic influences on the east asian weather. *Sci-*
 472 *entific Reports*, *9*(1), 7865. Retrieved from [https://doi.org/10.1038/s41598-](https://doi.org/10.1038/s41598-019-44414-w)
 473 [-019-44414-w](https://doi.org/10.1038/s41598-019-44414-w) doi: [10.1038/s41598-019-44414-w](https://doi.org/10.1038/s41598-019-44414-w)
- 474 CMIP5. (2012). "Coupled Model Intercomparison Project 5 (CMIP5) [Dataset]". Re-
 475 trieved from <https://esgf-node.llnl.gov/projects/cmip5/>
- 476 CMIP6. (2016). "Coupled Model Intercomparison Project 6 (CMIP6) [Dataset]". Re-
 477 trieved from <https://esgf-node.llnl.gov/projects/cmip6/>
- 478 Coumou, D., Di Capua, G., Vavrus, S., Wang, L., & Wang, S. (2018). The influ-
 479 ence of arctic amplification on mid-latitude summer circulation. *Nature Com-*
 480 *munications*, *9*(1), 2959. Retrieved from [https://doi.org/10.1038/s41467-](https://doi.org/10.1038/s41467-018-05256-8)
 481 [-018-05256-8](https://doi.org/10.1038/s41467-018-05256-8) doi: [10.1038/s41467-018-05256-8](https://doi.org/10.1038/s41467-018-05256-8)
- 482 Dai, Y., Feldstein, S. B., Tan, B., & Lee, S. (2017). Formation mechanisms of
 483 the pacific–north american teleconnection with and without its canonical
 484 tropical convection pattern. *Journal of Climate*, *30*(9), 3139–3155. Re-
 485 trieved from [https://journals.ametsoc.org/view/journals/clim/30/9/](https://journals.ametsoc.org/view/journals/clim/30/9/jcli-d-16-0411.1.xml)
 486 [jcli-d-16-0411.1.xml](https://journals.ametsoc.org/view/journals/clim/30/9/jcli-d-16-0411.1.xml) doi: <https://doi.org/10.1175/JCLI-D-16-0411.1>
- 487 Ding, S., Chen, W., Graf, H.-F., Guo, Y., & Nath, D. (2018). Distinct winter pat-
 488 terns of tropical pacific convection anomaly and the associated extratropical
 489 wave trains in the northern hemisphere. *Climate Dynamics*, *51*(5), 2003–
 490 2022. Retrieved from <https://doi.org/10.1007/s00382-017-3995-0> doi:
 491 [10.1007/s00382-017-3995-0](https://doi.org/10.1007/s00382-017-3995-0)
- 492 Duan, A., Sun, R., & He, J. (2017). Impact of surface sensible heating over the
 493 tibetan plateau on the western pacific subtropical high: A land–air–sea in-
 494 teraction perspective. *Advances in Atmospheric Sciences*, *34*(2), 157–168.
 495 Retrieved from <https://doi.org/10.1007/s00376-016-6008-z> doi:
 496 [10.1007/s00376-016-6008-z](https://doi.org/10.1007/s00376-016-6008-z)
- 497 Emanuel, K. A., David Neelin, J., & Bretherton, C. S. (1994, 2023/04/04). On
 498 large-scale circulations in convecting atmospheres. *Quarterly Journal of*
 499 *the Royal Meteorological Society*, *120*(519), 1111–1143. Retrieved from
 500 <https://doi.org/10.1002/qj.49712051902> doi: [https://doi.org/10.1002/](https://doi.org/10.1002/qj.49712051902)
 501 [qj.49712051902](https://doi.org/10.1002/qj.49712051902)
- 502 Fereday, D. R., Chadwick, R., Knight, J. R., & Scaife, A. A. (2020, 2023/04/04).
 503 Tropical rainfall linked to stronger future enso-nao teleconnection in cmip5
 504 models. *Geophysical Research Letters*, *47*(22), e2020GL088664. Retrieved from
 505 <https://doi.org/10.1029/2020GL088664> doi: [https://doi.org/10.1029/](https://doi.org/10.1029/2020GL088664)

2020GL088664

- 506 Franzke, C., Feldstein, S. B., & Lee, S. (2011, 2023/04/05). Synoptic analysis of the
507 pacific–north american teleconnection pattern. *Quarterly Journal of the Royal*
508 *Meteorological Society*, *137*(655), 329–346. Retrieved from [https://doi.org/](https://doi.org/10.1002/qj.768)
509 [10.1002/qj.768](https://doi.org/10.1002/qj.768) doi: <https://doi.org/10.1002/qj.768>
- 510 Gan, B., & Wu, L. (2012). Modulation of atmospheric response to north pacific
511 sst anomalies under global warming: A statistical assessment. *Journal of Cli-*
512 *mate*, *25*(19), 6554–6566. Retrieved from [https://journals.ametsoc.org/](https://journals.ametsoc.org/view/journals/clim/25/19/jcli-d-11-00493.1.xml)
513 [view/journals/clim/25/19/jcli-d-11-00493.1.xml](https://journals.ametsoc.org/view/journals/clim/25/19/jcli-d-11-00493.1.xml) doi: [https://doi.org/](https://doi.org/10.1175/JCLI-D-11-00493.1)
514 [10.1175/JCLI-D-11-00493.1](https://doi.org/10.1175/JCLI-D-11-00493.1)
- 515 Gill, A. E. (1980, 2023/03/22). Some simple solutions for heat-induced tropical
516 circulation. *Quarterly Journal of the Royal Meteorological Society*, *106*(449),
517 447–462. Retrieved from <https://doi.org/10.1002/qj.49710644905> doi:
518 <https://doi.org/10.1002/qj.49710644905>
- 519 Hagos, S., Zhang, C., Tao, W.-K., Lang, S., Takayabu, Y. N., Shige, S., ...
520 L'Ecuyer, T. (2010). Estimates of tropical diabatic heating profiles: Com-
521 monalities and uncertainties. *Journal of Climate*, *23*(3), 542–558. Re-
522 trieved from [https://journals.ametsoc.org/view/journals/clim/23/](https://journals.ametsoc.org/view/journals/clim/23/3/2009jcli3025.1.xml)
523 [3/2009jcli3025.1.xml](https://journals.ametsoc.org/view/journals/clim/23/3/2009jcli3025.1.xml) doi: <https://doi.org/10.1175/2009JCLI3025.1>
- 524 He, C., & Zhou, T. (2014). The two interannual variability modes of the western
525 north pacific subtropical high simulated by 28 cmip5–amip models. *Climate*
526 *Dynamics*, *43*(9), 2455–2469. Retrieved from [https://doi.org/10.1007/](https://doi.org/10.1007/s00382-014-2068-x)
527 [s00382-014-2068-x](https://doi.org/10.1007/s00382-014-2068-x) doi: [10.1007/s00382-014-2068-x](https://doi.org/10.1007/s00382-014-2068-x)
- 528 He, C., & Zhou, T. (2015). Responses of the western north pacific subtropical high
529 to global warming under rcp4.5 and rcp8.5 scenarios projected by 33 cmip5
530 models: The dominance of tropical indian ocean–tropical western pacific sst
531 gradient. *Journal of Climate*, *28*(1), 365–380. Retrieved from [https://](https://journals.ametsoc.org/view/journals/clim/28/1/jcli-d-13-00494.1.xml)
532 journals.ametsoc.org/view/journals/clim/28/1/jcli-d-13-00494.1.xml
533 doi: <https://doi.org/10.1175/JCLI-D-13-00494.1>
- 534 He, J., & Soden, B. J. (2015). Anthropogenic weakening of the tropical circu-
535 lation: The relative roles of direct co2 forcing and sea surface temperature
536 change. *Journal of Climate*, *28*(22), 8728–8742. Retrieved from [https://](https://journals.ametsoc.org/view/journals/clim/28/22/jcli-d-15-0205.1.xml)
537 journals.ametsoc.org/view/journals/clim/28/22/jcli-d-15-0205.1.xml
538 doi: <https://doi.org/10.1175/JCLI-D-15-0205.1>
- 539 He, J., Soden, B. J., & Kirtman, B. (2014, 2023/05/08). The robustness of
540 the atmospheric circulation and precipitation response to future anthro-
541 pogenic surface warming. *Geophysical Research Letters*, *41*(7), 2614–
542 2622. Retrieved from <https://doi.org/10.1002/2014GL059435> doi:
543 <https://doi.org/10.1002/2014GL059435>
- 544 Held, I. M., Ting, M., & Wang, H. (2002). Northern winter stationary waves:
545 Theory and modeling. *Journal of Climate*, *15*(16), 2125–2144. Retrieved
546 from [https://journals.ametsoc.org/view/journals/clim/15/16/](https://journals.ametsoc.org/view/journals/clim/15/16/1520-0442.2002.015.2125_nswta.2.0.co.2.xml)
547 [1520-0442.2002.015.2125_nswta.2.0.co.2.xml](https://journals.ametsoc.org/view/journals/clim/15/16/1520-0442.2002.015.2125_nswta.2.0.co.2.xml) doi: [https://doi.org/](https://doi.org/10.1175/1520-0442(2002)015(2125:NWSWTA)2.0.CO;2)
548 [10.1175/1520-0442\(2002\)015\(2125:NWSWTA\)2.0.CO;2](https://doi.org/10.1175/1520-0442(2002)015(2125:NWSWTA)2.0.CO;2)
- 549 Hoskins, B. J., James, I. N., & White, G. H. (1983). The shape, propagation
550 and mean-flow interaction of large-scale weather systems. *Journal of At-*
551 *mospheric Sciences*, *40*(7), 1595 - 1612. Retrieved from [https://journals](https://journals.ametsoc.org/view/journals/atsc/40/7/1520-0469.1983.040.1595.tspamf_2.0.co.2.xml)
552 [.ametsoc.org/view/journals/atsc/40/7/1520-0469.1983.040.1595.tspamf](https://journals.ametsoc.org/view/journals/atsc/40/7/1520-0469.1983.040.1595.tspamf_2.0.co.2.xml)
553 [_2.0.co.2.xml](https://journals.ametsoc.org/view/journals/atsc/40/7/1520-0469.1983.040.1595.tspamf_2.0.co.2.xml) doi: [https://doi.org/10.1175/1520-0469\(1983\)040\(1595:](https://doi.org/10.1175/1520-0469(1983)040(1595:TSPAMF)2.0.CO;2)
554 [TSPAMF\)2.0.CO;2](https://doi.org/10.1175/1520-0469(1983)040(1595:TSPAMF)2.0.CO;2)
- 555 Huang, D., Liu, A., Zheng, Y., & Zhu, J. (2022, 2023/03/23). Inter-model spread
556 of the simulated east asian summer monsoon rainfall and the associated atmo-
557 spheric circulations from the cmip6 models. *Journal of Geophysical Research:*
558 *Atmospheres*, *127*(20), e2022JD037371. Retrieved from [https://doi.org/](https://doi.org/10.1029/2022JD037371)
559 [10.1029/2022JD037371](https://doi.org/10.1029/2022JD037371) doi: <https://doi.org/10.1029/2022JD037371>
- 560

- 561 Huang, P., Xie, S.-P., Hu, K., Huang, G., & Huang, R. (2013). Patterns of the sea-
562 sonal response of tropical rainfall to global warming. *Nature Geoscience*, *6*(5),
563 357–361. Retrieved from <https://doi.org/10.1038/ngeo1792> doi: 10.1038/
564 ngeo1792
- 565 Hurrell, J. W., Holland, M. M., Gent, P. R., Ghan, S., Kay, J. E., Kushner, P. J.,
566 ... Marshall, S. (2013). The community earth system model: A framework
567 for collaborative research. *Bulletin of the American Meteorological Society*,
568 *94*(9), 1339–1360. Retrieved from [https://journals.ametsoc.org/view/
569 journals/bams/94/9/bams-d-12-00121.1.xml](https://journals.ametsoc.org/view/journals/bams/94/9/bams-d-12-00121.1.xml) doi: [https://doi.org/10.1175/
570 BAMS-D-12-00121.1](https://doi.org/10.1175/BAMS-D-12-00121.1)
- 571 Kay, J. E., Deser, C., Phillips, A., Mai, A., Hannay, C., Strand, G., ... Verten-
572 stein, M. (2015). The community earth system model (cesm) large ensemble
573 project: A community resource for studying climate change in the presence of
574 internal climate variability. *Bulletin of the American Meteorological Society*,
575 *96*(8), 1333–1349. Retrieved from [https://journals.ametsoc.org/view/
576 journals/bams/96/8/bams-d-13-00255.1.xml](https://journals.ametsoc.org/view/journals/bams/96/8/bams-d-13-00255.1.xml) doi: [https://doi.org/10.1175/
577 BAMS-D-13-00255.1](https://doi.org/10.1175/BAMS-D-13-00255.1)
- 578 Kosaka, Y., Xie, S.-P., Lau, N.-C., & Vecchi, G. A. (2013, 2023/03/16). Ori-
579 gin of seasonal predictability for summer climate over the northwestern
580 pacific. *Proceedings of the National Academy of Sciences*, *110*(19), 7574–
581 7579. Retrieved from <https://doi.org/10.1073/pnas.1215582110> doi:
582 10.1073/pnas.1215582110
- 583 Levine, X. J., & Boos, W. R. (2017, 2023/03/01). Land surface albedo bias in cli-
584 mate models and its association with tropical rainfall. *Geophysical Research
585 Letters*, *44*(12), 6363–6372. Retrieved from [https://doi.org/10.1002/
586 2017GL072510](https://doi.org/10.1002/2017GL072510) doi: <https://doi.org/10.1002/2017GL072510>
- 587 Levine, X. J., & Boos, W. R. (2019). Sensitivity of subtropical stationary circu-
588 lations to global warming in climate models: a baroclinic rossby gyre theory.
589 *Climate Dynamics*, *52*(7), 4873–4890. Retrieved from [https://doi.org/
590 10.1007/s00382-018-4419-5](https://doi.org/10.1007/s00382-018-4419-5) doi: 10.1007/s00382-018-4419-5
- 591 Li, W., Li, L., Ting, M., & Liu, Y. (2012). Intensification of northern hemi-
592 sphere subtropical highs in a warming climate. *Nature Geoscience*, *5*(11),
593 830–834. Retrieved from <https://doi.org/10.1038/ngeo1590> doi:
594 10.1038/ngeo1590
- 595 Lindzen, R. S., & Nigam, S. (1987). On the role of sea surface tempera-
596 ture gradients in forcing low-level winds and convergence in the trop-
597 ics. *Journal of Atmospheric Sciences*, *44*(17), 2418–2436. Retrieved
598 from [https://journals.ametsoc.org/view/journals/atsc/44/17/
599 1520-0469_1987_044_2418_otross_2_0_co_2.xml](https://journals.ametsoc.org/view/journals/atsc/44/17/1520-0469_1987_044_2418_otross_2_0_co_2.xml) doi: [https://doi.org/
600 10.1175/1520-0469\(1987\)044<2418:OTROSS>2.0.CO;2](https://doi.org/10.1175/1520-0469(1987)044<2418:OTROSS>2.0.CO;2)
- 601 Lu, K., He, J., & Simpson, I. (2023, June). "Origins of Uncertainty in Projections
602 of Summer North Pacific Subtropical High [Dataset]". Zenodo. Retrieved from
603 <https://doi.org/10.5281/zenodo.8327817> doi: 10.5281/zenodo.8327817
- 604 Matsuno, T. (1966). Quasi-geostrophic motions in the equatorial area. *Jour-
605 nal of the Meteorological Society of Japan. Ser. II*, *44*(1), 25–43. doi: 10.2151/
606 jmsj1965.44.1{-}25
- 607 Mauritsen, T., & Stevens, B. (2015). Missing iris effect as a possible cause of muted
608 hydrological change and high climate sensitivity in models. *Nature Geoscience*,
609 *8*(5), 346–351. Retrieved from <https://doi.org/10.1038/ngeo2414> doi: 10
610 .1038/ngeo2414
- 611 Mestas-Nuñez, A. M. (2000). Orthogonality properties of rotated empirical
612 modes. *International Journal of Climatology*, *20*(12), 1509–1516. Re-
613 trieved from [https://rmets.onlinelibrary.wiley.com/doi/abs/10.1002/
614 1097-0088%28200010%2920%3A12%3C1509%3A%3AAID-JOC553%3E3.O.CO%3B2-Q](https://rmets.onlinelibrary.wiley.com/doi/abs/10.1002/1097-0088%28200010%2920%3A12%3C1509%3A%3AAID-JOC553%3E3.O.CO%3B2-Q)
615 doi: [https://doi.org/10.1002/1097-0088\(200010\)20:12<1509::AID-JOC553>3.0](https://doi.org/10.1002/1097-0088(200010)20:12<1509::AID-JOC553>3.0)

- 616 .CO;2-Q
- 617 O'Neill, B. C., Tebaldi, C., van Vuuren, D. P., Eyring, V., Friedlingstein, P., Hurtt,
618 G., . . . Sanderson, B. M. (2016). The scenario model intercomparison project
619 (scenariomip) for cmip6. *Geoscientific Model Development*, *9*(9), 3461–3482.
620 Retrieved from <https://gmd.copernicus.org/articles/9/3461/2016/> doi:
621 10.5194/gmd-9-3461-2016
- 622 Park, M., & Lee, S. (2021, 2023/01/20). Is the stationary wave bias in cmip5 simu-
623 lations driven by latent heating biases? *Geophysical Research Letters*, *48*(4),
624 e2020GL091678. Retrieved from <https://doi.org/10.1029/2020GL091678>
625 doi: <https://doi.org/10.1029/2020GL091678>
- 626 Portal, A., Pasquero, C., D'Andrea, F., Davini, P., Hamouda, M. E., & Rivière,
627 G. (2022). Influence of reduced winter land–sea contrast on the midlati-
628 tude atmospheric circulation. *Journal of Climate*, *35*(19), 2637–2651. Re-
629 trieved from [https://journals.ametsoc.org/view/journals/clim/35/19/](https://journals.ametsoc.org/view/journals/clim/35/19/JCLI-D-21-0941.1.xml)
630 [JCLI-D-21-0941.1.xml](https://journals.ametsoc.org/view/journals/clim/35/19/JCLI-D-21-0941.1.xml) doi: <https://doi.org/10.1175/JCLI-D-21-0941.1>
- 631 Rodwell, M. J., & Hoskins, B. J. (2001). Subtropical anticyclones and sum-
632 mer monsoons. *Journal of Climate*, *14*(15), 3192–3211. Retrieved
633 from [https://journals.ametsoc.org/view/journals/clim/14/15/](https://journals.ametsoc.org/view/journals/clim/14/15/1520-0442_2001_014_3192_saasm_2.0.co_2.xml)
634 [1520-0442_2001_014_3192_saasm_2.0.co_2.xml](https://journals.ametsoc.org/view/journals/clim/14/15/1520-0442_2001_014_3192_saasm_2.0.co_2.xml) doi: [https://doi.org/10.1175/](https://doi.org/10.1175/1520-0442(2001)014(3192:SAASM)2.0.CO;2)
635 [1520-0442\(2001\)014\(3192:SAASM\)2.0.CO;2](https://doi.org/10.1175/1520-0442(2001)014(3192:SAASM)2.0.CO;2)
- 636 Seager, R., Osborn, T. J., Kushnir, Y., Simpson, I. R., Nakamura, J., & Liu,
637 H. (2019). Climate variability and change of mediterranean-type cli-
638 mates. *Journal of Climate*, *32*(10), 2887–2915. Retrieved from [https://](https://journals.ametsoc.org/view/journals/clim/32/10/jcli-d-18-0472.1.xml)
639 journals.ametsoc.org/view/journals/clim/32/10/jcli-d-18-0472.1.xml
640 doi: <https://doi.org/10.1175/JCLI-D-18-0472.1>
- 641 Shaw, T. A., & Voigt, A. (2015). Tug of war on summertime circulation be-
642 tween radiative forcing and sea surface warming. *Nature Geoscience*, *8*(7),
643 560–566. Retrieved from <https://doi.org/10.1038/ngeo2449> doi:
644 [10.1038/ngeo2449](https://doi.org/10.1038/ngeo2449)
- 645 Sigmond, M., Kushner, P. J., & Scinocca, J. F. (2007, 2023/01/02). Discriminating
646 robust and non-robust atmospheric circulation responses to global warming.
647 *Journal of Geophysical Research: Atmospheres*, *112*(D20). Retrieved from
648 <https://doi.org/10.1029/2006JD008270> doi: [https://doi.org/10.1029/](https://doi.org/10.1029/2006JD008270)
649 [2006JD008270](https://doi.org/10.1029/2006JD008270)
- 650 Su, H., Jiang, J. H., Neelin, J. D., Shen, T. J., Zhai, C., Yue, Q., . . . Yung, Y. L.
651 (2017). Tightening of tropical ascent and high clouds key to precipitation
652 change in a warmer climate. *Nature Communications*, *8*(1), 15771. Retrieved
653 from <https://doi.org/10.1038/ncomms15771> doi: [10.1038/ncomms15771](https://doi.org/10.1038/ncomms15771)
- 654 Sui, C.-H., Chung, P.-H., & Li, T. (2007, 2023/03/03). Interannual and interdecadal
655 variability of the summertime western north pacific subtropical high. *Geophys-
656 ical Research Letters*, *34*(11). Retrieved from [https://doi.org/10.1029/](https://doi.org/10.1029/2006GL029204)
657 [2006GL029204](https://doi.org/10.1029/2006GL029204) doi: <https://doi.org/10.1029/2006GL029204>
- 658 Takaya, K., & Nakamura, H. (1997, 2023/03/24). A formulation of a wave-activity
659 flux for stationary rossby waves on a zonally varying basic flow. *Geophys-
660 ical Research Letters*, *24*(23), 2985–2988. Retrieved from [https://doi.org/](https://doi.org/10.1029/97GL03094)
661 [10.1029/97GL03094](https://doi.org/10.1029/97GL03094) doi: <https://doi.org/10.1029/97GL03094>
- 662 Taylor, K. E., Stouffer, R. J., & Meehl, G. A. (2012). An overview of cmip5 and
663 the experiment design. *Bulletin of the American Meteorological Society*, *93*(4),
664 485–498. Retrieved from [https://journals.ametsoc.org/view/journals/](https://journals.ametsoc.org/view/journals/bams/93/4/bams-d-11-00094.1.xml)
665 [bams/93/4/bams-d-11-00094.1.xml](https://journals.ametsoc.org/view/journals/bams/93/4/bams-d-11-00094.1.xml) doi: [https://doi.org/10.1175/BAMS-D-](https://doi.org/10.1175/BAMS-D-11-00094.1)
666 [11-00094.1](https://doi.org/10.1175/BAMS-D-11-00094.1)
- 667 Ting, M., Wang, H., & Yu, L. (2001). Nonlinear stationary wave maintenance
668 and seasonal cycle in the gfdl r30 gcm. *Journal of the Atmospheric Sciences*,
669 *58*(16), 2331–2354. Retrieved from [https://journals.ametsoc.org/view/](https://journals.ametsoc.org/view/journals/atsc/58/16/1520-0469_2001_058_2331_nswmas_2.0.co_2.xml)
670 [journals/atsc/58/16/1520-0469_2001_058_2331_nswmas_2.0.co_2.xml](https://journals.ametsoc.org/view/journals/atsc/58/16/1520-0469_2001_058_2331_nswmas_2.0.co_2.xml) doi:

- 10.1175/1520-0469(2001)058<2331:NSWMAS>2.0.CO;2
- 671 Ting, M., & Yu, L. (1998). Steady response to tropical heating in wavy lin-
 672 ear and nonlinear baroclinic models. *Journal of the Atmospheric Sciences*,
 673 55(24), 3565–3582. Retrieved from [https://journals.ametsoc.org/view/
 674 journals/atsc/55/24/1520-0469_1998_055_3565_srtthi.2.0.co.2.xml](https://journals.ametsoc.org/view/journals/atsc/55/24/1520-0469_1998_055_3565_srtthi.2.0.co.2.xml) doi:
 675 [https://doi.org/10.1175/1520-0469\(1998\)055<3565:SRTTHI>2.0.CO;2](https://doi.org/10.1175/1520-0469(1998)055<3565:SRTTHI>2.0.CO;2)
 676
- 677 Wang, B., Xiang, B., & Lee, J.-Y. (2013, 2023/03/25). Subtropical high pre-
 678 dictability establishes a promising way for monsoon and tropical storm pre-
 679 dictions. *Proceedings of the National Academy of Sciences*, 110(8), 2718–
 680 2722. Retrieved from <https://doi.org/10.1073/pnas.1214626110> doi:
 681 [10.1073/pnas.1214626110](https://doi.org/10.1073/pnas.1214626110)
- 682 Wang, X., Xie, S.-P., Guan, Z., & Wang, M. (2021). A common base mode of
 683 asian summer monsoon variability across timescales. *Journal of Climate*,
 684 34(18), 7359 - 7371. Retrieved from [https://journals.ametsoc.org/view/
 685 journals/clim/34/18/JCLI-D-20-0856.1.xml](https://journals.ametsoc.org/view/journals/clim/34/18/JCLI-D-20-0856.1.xml) doi: [https://doi.org/10.1175/
 686 JCLI-D-20-0856.1](https://doi.org/10.1175/JCLI-D-20-0856.1)
- 687 Wang, Y., Wu, B., & Zhou, T. (2022). Maintenance of western north pacific anoma-
 688 lous anticyclone in boreal summer by wind-induced moist enthalpy advection
 689 mechanism. *Journal of Climate*, 35(14), 4499–4511. Retrieved from [https://
 690 journals.ametsoc.org/view/journals/clim/35/14/JCLI-D-21-0708.1.xml](https://journals.ametsoc.org/view/journals/clim/35/14/JCLI-D-21-0708.1.xml) doi: <https://doi.org/10.1175/JCLI-D-21-0708.1>
 691
- 692 Weare, B. C., Navato, A. R., & Newell, R. E. (1976). Empirical orthogonal analy-
 693 sis of pacific sea surface temperatures. *Journal of Physical Oceanography*, 6(5),
 694 671–678. Retrieved from [https://journals.ametsoc.org/view/journals/
 695 phoc/6/5/1520-0485_1976_006_0671_eoaops.2.0.co.2.xml](https://journals.ametsoc.org/view/journals/phoc/6/5/1520-0485_1976_006_0671_eoaops.2.0.co.2.xml) doi: [https://doi/
 696 .org/10.1175/1520-0485\(1976\)006<0671:EOAOPS>2.0.CO;2](https://doi.org/10.1175/1520-0485(1976)006<0671:EOAOPS>2.0.CO;2)
- 697 Webb, M. J., Andrews, T., Bodas-Salcedo, A., Bony, S., Bretherton, C. S., Chad-
 698 wick, R., ... Watanabe, M. (2017). The cloud feedback model intercomparison
 699 project (cfmip) contribution to cimp6. *Geoscientific Model Development*,
 700 10(1), 359–384. Retrieved from [https://gmd.copernicus.org/articles/10/
 701 359/2017/](https://gmd.copernicus.org/articles/10/359/2017/) doi: [10.5194/gmd-10-359-2017](https://doi.org/10.5194/gmd-10-359-2017)
- 702 Wills, R. C. J., White, R. H., & Levine, X. J. (2019). Northern hemisphere station-
 703 ary waves in a changing climate. *Current Climate Change Reports*, 5(4), 372–
 704 389. Retrieved from <https://doi.org/10.1007/s40641-019-00147-6> doi: [10
 705 .1007/s40641-019-00147-6](https://doi.org/10.1007/s40641-019-00147-6)
- 706 Wu, B., Zhou, T., & Li, T. (2017). Atmospheric dynamic and thermodynamic
 707 processes driving the western north pacific anomalous anticyclone during el
 708 niño. part i: Maintenance mechanisms. *Journal of Climate*, 30(23), 9621–9635.
 709 Retrieved from [https://journals.ametsoc.org/view/journals/clim/30/
 710 23/jcli-d-16-0489.1.xml](https://journals.ametsoc.org/view/journals/clim/30/23/jcli-d-16-0489.1.xml) doi: <https://doi.org/10.1175/JCLI-D-16-0489.1>
- 711 Xie, S.-P., Deser, C., Vecchi, G. A., Ma, J., Teng, H., & Wittenberg, A. T. (2010a).
 712 Global warming pattern formation: Sea surface temperature and rainfall. *Jour-
 713 nal of Climate*, 23(4), 966 - 986. Retrieved from [https://journals.ametsoc
 714 .org/view/journals/clim/23/4/2009jcli3329.1.xml](https://journals.ametsoc.org/view/journals/clim/23/4/2009jcli3329.1.xml) doi: [https://doi.org/
 715 10.1175/2009JCLI3329.1](https://doi.org/10.1175/2009JCLI3329.1)
- 716 Xie, S.-P., Deser, C., Vecchi, G. A., Ma, J., Teng, H., & Wittenberg, A. T. (2010b).
 717 Global warming pattern formation: Sea surface temperature and rainfall. *Jour-
 718 nal of Climate*, 23(4), 966–986. Retrieved from [https://journals.ametsoc
 719 .org/view/journals/clim/23/4/2009jcli3329.1.xml](https://journals.ametsoc.org/view/journals/clim/23/4/2009jcli3329.1.xml) doi: [https://doi.org/
 720 10.1175/2009JCLI3329.1](https://doi.org/10.1175/2009JCLI3329.1)
- 721 Xie, S.-P., Hu, K., Hafner, J., Tokinaga, H., Du, Y., Huang, G., & Sampe, T.
 722 (2009). Indian ocean capacitor effect on indo-western pacific climate dur-
 723 ing the summer following el niño. *Journal of Climate*, 22(3), 730–747. Re-
 724 trieved from [https://journals.ametsoc.org/view/journals/clim/22/3/
 725 2008jcli2544.1.xml](https://journals.ametsoc.org/view/journals/clim/22/3/2008jcli2544.1.xml) doi: [10.1175/2008JCLI2544.1](https://doi.org/10.1175/2008JCLI2544.1)

- 726 Zhou, S., Huang, P., Huang, G., & Hu, K. (2019). Leading source and constraint
727 on the systematic spread of the changes in east asian and western north pacific
728 summer monsoon. , *14*(12), 124059. Retrieved from [https://dx.doi.org/](https://dx.doi.org/10.1088/1748-9326/ab547c)
729 [10.1088/1748-9326/ab547c](https://dx.doi.org/10.1088/1748-9326/ab547c) doi: 10.1088/1748-9326/ab547c
730 Zhou, W., & Xie, S.-P. (2017, 2023/04/04). Intermodel spread of the double-itcz
731 bias in coupled gcms tied to land surface temperature in amip gcms. *Geophys-*
732 *ical Research Letters*, *44*(15), 7975–7984. Retrieved from [https://doi.org/10](https://doi.org/10.1002/2017GL074377)
733 [.1002/2017GL074377](https://doi.org/10.1002/2017GL074377) doi: <https://doi.org/10.1002/2017GL074377>